PAPER • **OPEN ACCESS**

Controlling the electronic properties of van der Waals heterostructures by applying electrostatic design

To cite this article: Christian Winkler *et al* 2018 *2D Mater.* **5** 035019

View the article online for updates and enhancements.

Related content

- Calculating excitons, plasmons, and quasiparticles in 2D materials and van der Waals heterostructures
  Kristian Sommer Thygesen
- Van der Waals stacked 2D layered materials for optoelectronics
  Wenjing Zhang, Qixing Wang, Yu Chen et al.
- Light–matter interaction in transition metal dichalcogenides and their heterostructures
  Ursula Wurstbauer, Bastian Miller, Eric Parzinger et al.

IOP ebooks™

Bringing you innovative digital publishing with leading voices to create your essential collection of books in STEM research.

Start exploring the collection - download the first chapter of every title for free.

This content was downloaded from IP address 129.11.22.227 on 20/11/2018 at 16:09

2D Materials

OPEN ACCESS

RECEIVED
15 December 2017

REVISED
3 April 2018

ACCEPTED FOR PUBLICATION
17 April 2018

PUBLISHED
11 May 2018

Original content from this work may be used under the terms of the Creative Commons Attribution 3.0 licence.

Any further distribution of this work must maintain attribution to the author(s) and the title of the work, journal citation and DOI.

PAPER

Controlling the electronic properties of van der Waals heterostructures by applying electrostatic design

Christian Winkler, Shashank S Harivyasi and Egbert Zojer

Institute of Solid State Physics, NAWI Graz, Graz University of Technology, Petersgasse 16, 8010 Graz, Austria

E-mail: egbert.zojer@tugraz.at

Keywords: van der Waals heterostructures, transition-metal dichalcogenides, electrostatic design, band alignment, quantum well, quantum cascade, density functional theory

Supplementary material for this article is available online

Abstract

Van der Waals heterostructures based on the heteroassembly of 2D materials represent a recently developed class of materials with promising properties especially for optoelectronic applications. The alignment of electronic energy bands between consecutive layers of these heterostructures crucially determines their functionality. In the present paper, relying on dispersion-corrected density-functional theory calculations, we present electrostatic design as a promising tool for manipulating this band alignment. The latter is achieved by inserting a layer of aligned polar molecules between consecutive transition-metal dichalcogenide (TMD) sheets. As a consequence, collective electrostatic effects induce a shift of as much as 0.3 eV in the band edges of successive TMD layers. Building on that, the proposed approach can be used to design electronically more complex systems, like quantum cascades or quantum wells, or to change the type of band lineup between type II and type I.

1. Introduction

Research on two-dimensional (2D) materials has been growing rapidly since the successful exfoliation of graphene [1]. Nowadays the full range of electronic properties can be realized in various classes of 2D materials. Amongst them, semiconducting transition-metal dichalcogenides (TMDs) have proven to be especially interesting, on the one hand, for gaining fundamental physical insights and, on the other hand, for optoelectronic applications. This is associated with the emergence of spin and valley physics [2–4] and strong light–matter interactions [5–7] observed in these systems. The latter result in large absorption coefficients and, for properly designed band-offsets, either in significant electron–hole pair creation or exciton recombination, two properties highly relevant for optoelectronics. Of particular interest in this context is the combination of semiconducting organic molecules with 2D materials to change their characteristics either via doping [8, 9] or by the exploitation of dielectric effects [10].

In their monolayer form, the TMDs in the focus of the present paper [MoX_2 and WX_2 (X = S, Se)] have a direct band gap ranging between 2.0 to 2.5 eV [11]. Additionally, the exciton binding energies [11–14] of these layered semiconductors are an order of magnitude larger than in conventional bulk semiconductors such as Si or GaAs resulting in an increased stability of the excitons against thermal dissociation. As a consequence, the strongly bound excitons of MoX_2 and WX_2 have been shown to be stable at room temperature [15–17]. This makes TMD monolayers promising candidates for optoelectronics. Even more interesting are vdW heterostructures [15, 18–20], which consist of different TMD layers stacked on top of each other along the direction perpendicular to the 2D plane. Individual layers in such vdW heterostructures are held together by strong in-plane covalent bonds, while comparably weak vdW interactions are present between the layers. Because of this weak interlayer bonding, 2D crystals with different lattice constants and crystal structures can be easily combined to form vdW heterostructures, which are chemically stable, flexible [21, 22] and have atomically sharp interfaces. Consequently, it is easy to mix and match 2D materials with different electronic properties such as semiconductors (e.g. TMDs), semimetals (e.g. graphene) or insulators (e.g. hexagonal boron nitride). In the resulting structures, the variation of the charac-

© 2018 IOP Publishing Ltd

teristics of individual layers can be exploited to create new types of devices.

A crucial property that determines the functionality of van der Waals heterostructures is the alignment of the valence band maxima (referred hereafter as VBM) and conduction band minima (CBM) of consecutive layers. For example, to obtain TMD-based heterobilayer systems that promote charge carrier separation, the band extrema of the two TMD layers should have type II band lineup with a sufficiently large band offset to overcome the exciton binding energy; otherwise the system would fail to localize charge carriers onto the two layers as is shown in figure 1(a). Consequently, in order to realize a functional vdW heterostructure with specific properties, one possibility would be to search the available pool of 2D materials [23] for a combination of layers, where the sizes of the band gaps and the band lineup suite the intended purpose. This can be tedious and sometimes requires the application of materials that are difficult to obtain/handle.

Therefore, in this paper, we suggest an alternative approach for tuning the band alignment of vdW heterostructures, which is based on electrostatic design. This concept has been introduced by Kretz *et al* [24] for controlling the energetics of the electronic states of self-assembled organic monolayers (SAMs). Later it has been applied to modify the electronic structure of graphene [25]. The approach relies on collective electrostatic effects, which arise from a regular and periodic arrangement of dipolar groups in an organic monolayer resulting in a step in the energy landscape [26–31]. In the present paper, we show that this design principle holds high promise for vdW heterostructures. In particular we discuss, how the intercalation of a monolayer consisting of oriented polar organic molecules triggers a step in the electrostatic energy, which leads to a shift between the electronic states of the TMD layers above, respectively, below the molecules. The shift can then be employed to tune the electronic structure, which can, for example, be exploited for increasing the band-offsets in neighboring layers to a degree that exciton-dissociation becomes energetically favorable (see figure 1(b) in comparison to figure 1(a)). Alternatively, one can use electrostatic design to switch between type II band lineup favoring exciton dissociation (figure 1(c)) and type I band lineup promoting exciton recombination (figure 1(d)).

In the following, we use quantum mechanical modeling in the framework of dispersion corrected density-functional theory (DFT) to discuss the enormous potential of electrostatic design. First, we describe prototypical stacks consisting solely of MoS_2 layers. Subsequently, we present the possibility to electrostatically design more complex systems such as quantum cascades and quantum wells. Finally, we show how for a system consisting of WSe_2 and $MoSe_2$ the above-mentioned qualitative change in the band alignment from type II to type I can be achieved.

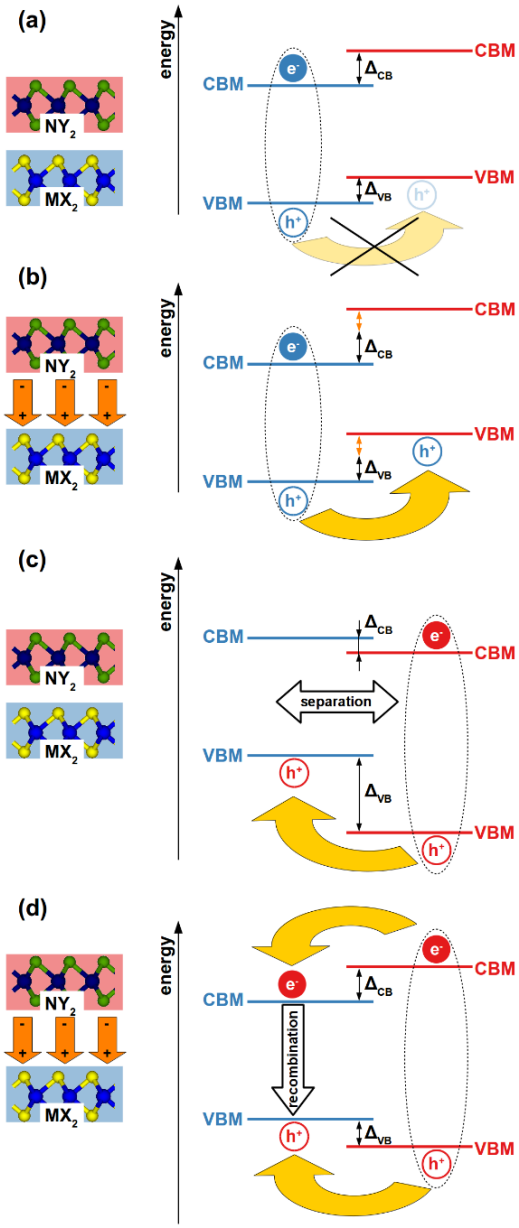

Figure 1. Electrostatic design applied to van der Waals (vdW) heterostructures. (a) vdW heterostructure consisting of two semiconducting TMDs which show symmetric type II band alignment (i.e. the valence- and conduction-band offsets are of equal magnitude and have the same sign). When the band offset of this system is too small, an intralayer exciton created in MX_2 cannot be separated. (b) When electrostatic design is applied to this heterostructure by inserting a polar layer, the bands of the upper TMD layer can be shifted and, thus, the band offsets (valence band offset Δ_{VB} and conduction band offset Δ_{CB}) can be changed. This promotes exciton dissociation. (c) van der Waals heterostructure with type II band alignment and very different band offsets (Δ_{VB} is much larger than Δ_{CB}). (d) By applying electrostatic design to such a heterostructure, the states of the upper layer can be shifted such that the band alignment changes from type II to type I (i.e. the signs of the valence- and conduction-band offsets differ).

2. Results and discussion

2.1. Choice and setup of the model system

The first system whose electronic properties are investigated contains only MoS_2 as 2D semiconducting

layers. As dipolar molecules intercalated between the MoS_2 sheets we chose titanyl-phthalocyanine (TiOPc; see inset in figure 2(c)) as a prototypical example. This choice is motivated by the observation of Fukagawa *et al* [32] that on weakly interacting substrates (explicitly shown for highly-oriented pyrolytic graphite, HOPG) up to monolayer coverage all TiOPc molecules align with their dipole moments pointing in the same direction (which is perpendicular to the HOPG surface). As a result, the work function of the sample continuously increases with coverage until a closed monolayer is formed. For that case, a work function modification of 0.29 eV is obtained in the experiment [32]. The observed arrangement of the molecules is a consequence of maximized van der Waals bonding when the Ti = O groups point away from the surface. Indeed, when fully relaxing the geometry of an MoS_2/TiOPc interface in the configuration shown in the supporting information (stacks.iop.org/TDM/5/035019/mmedia) the slightly bent molecular backbone is aligned essentially parallel to the substrate at a distance of 3.35 Å between the average planes of the topmost S layer and the C atoms. This results in a van der Waals attraction of 3.61 eV between the MoS_2 and the TiOPc. A configuration with the Ti = O group pointing towards the substrate would not only be at variance with the experimental observations on HOPG [32], we also calculate it to be less stable by 0.8 eV per molecule on MoS_2, which we attribute to a larger average distance between the substrate and the atoms in the molecular backbone. The experiments on HOPG also imply that the increased van der Waals attraction in the Ti = O up configuration is sufficient for overcoming intermolecular dipole–dipole repulsion between the molecules.

For the TiOPc intercalated van der Waals stack sketched in the inset of figure 2(c), no such driving force exists, as there are MoS_2 layers above and below the TiOPcs. Thus, the thermodynamically most stable configuration would be molecules aligned in an anti-parallel fashion. In the experiment, this problem can, however, be overcome by realizing a kinetically trapped configuration where first a TiOPc layer is deposited onto a MoS_2 surface and, subsequently, the (modified) TMD layer is covered with a second MoS_2 flake [33, 34]. For stabilizing the orientation of the molecules in the intercalated layer, an option would also be to substitute them with cross-linkable side groups.

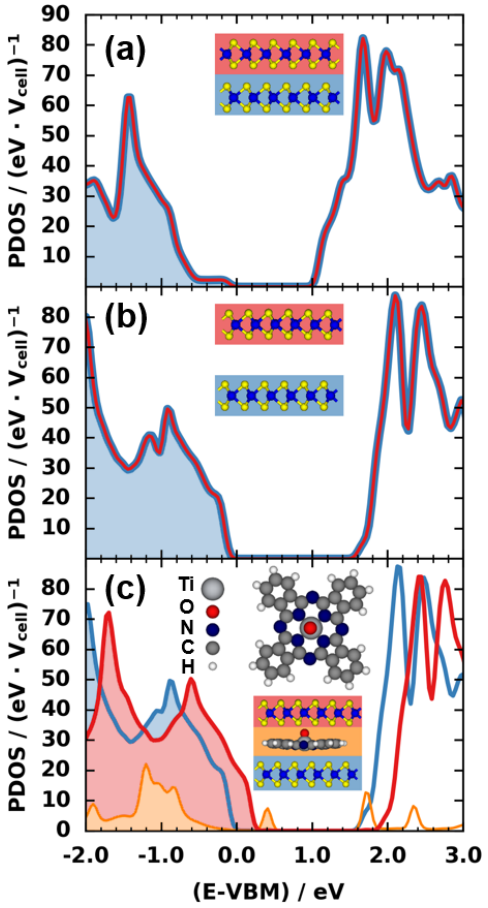

Figure 2. Density of states projected onto the different layers (PDOSs) in the MoS_2 based system (a) for the homobilayer (2H stacking), (b) for two MoS_2 layers arranged in the same geometry as in the intercalated stack, but in the absence of TiOPc molecules, and (c) in the stack containing a monolayer of dipolar TiOPcs. The structures of the considered stacks are shown as insets; note that the geometries of the systems depicted in panels (a) and (c) have been fully optimized. All energies are plotted relative to the valence band maximum of the bottom TMD layer for the sake of consistency; all shaded electronic states are occupied in the calculations (with details regarding the employed occupation smearing described in the Methods section. The inset in (c) shows the chemical structure of the TiOPc molecule.

2.2. Electronic structure of the MoS_2|TiOPc|MoS_2 system

To characterize the electronic structure of the investigated systems, it is particularly useful to discuss densities of states projected onto either individual TMD layers or onto the intercalated molecules (PDOSs); the corresponding band-structures can be found in the supporting information. The PDOS for a geometry relaxed bilayer system is shown in figure 2(a). Inserting the TiOPc layer slightly distorts especially the upper TMD layer, but, more, importantly also significantly increases the inter-layer distance. To highlight the consequences of these changes in the geometry of the TMD layers, figure 2(b) shows the PDOS of the system obtained when first relaxing the MoS_2|TiOPc|MoS_2 geometry (in a two-step process, for details see supporting information) and subsequently calculating the electronic properties of the stack with the TiOPc layer removed (figure 2(b)). In spite of the loss of mirror symmetry due to the buckling of the top layer, the densities of states projected onto the two MoS_2 monolayers still overlap. The differences between figures 2(a) and (b), especially in the region of the valence-band edge arise from quantum-mechanical interactions in the close-packed bilayer [35, 36]. They result in a plateau in the PDOS below the valence-band edge (figure 2(a)), which is

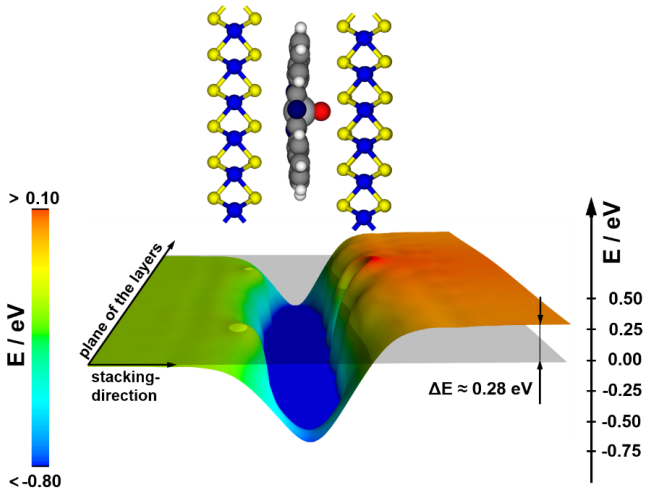

Figure 3. Surface plot of the change in the Hartree potential for the MoS_2|TiOPc|MoS_2 van der Waals heterostructure due to the presence of the molecular layer; to see the impact of the TiOPc layer, the difference between the Hartree potentials of the MoS_2|TiOPc|MoS_2 system with and without TiOPc is shown. The semi-transparent plane serves as a guide to the eye. In the region of the molecule the potential has been cut for values smaller than −0.80 eV.

fundamentally different from the steep increase of the DOS in the two separated monolayers (figure 2(b)), respectively, in an isolated monolayer (see supporting information). The reason for that is that the occupied states around the Γ point are dominated by p_z orbitals localized on S atoms and d_{z^2} orbitals on Mo [37] (see also species-projected DOS contained in the SI), whose 'out of plane' nature makes them particularly sensitive to inter-layer interactions. In the densely packed MoS_2 bilayer, this leads to a destabilization of the occupied electronic states around the Γ-point, resulting in an energy window, where only the highest occupied band is present (see supporting information). Its roughly parabolic shape then causes the small but constant DOS close to the VBM (see figure 2(a)) that is expected for a 2D electron gas. When the inter-layer spacing increases, as in figure 2(b), the coupling diminishes and a DOS essentially corresponding to that of an isolated monolayer is recovered.

The situation changes fundamentally in the MoS_2|TiOPc|MoS_2 heterostructure (see figure 2(c)). Here, one observes a shift of the band edges of the two MoS_2 layers, which is caused by the step in electrostatic energy due to the aligned TiOPc dipoles (see figure 3). The shift amounts to 0.28 eV, which is very close to the above-mentioned measured (calculated) work function change for TiOPc on HOPG amounting to 0.29 (0.30) eV [32]. This is consistent with the band offset being caused exclusively by the electrostatic shift induced by the TiOPc layer. This assessment is further supported by a vanishingly small bond-dipole (amounting to −0.01 eV) resulting from charge rearrangements upon interface formation. The particularly small value of the latter is primarily caused by a largely symmetric transfer of electrons from the TiOPc film to both MoS_2 layers. For a system with the top MoS_2 layer lifted by 0.5 Å, this symmetry is broken and a considerable net bond dipole of −0.09 eV is observed (see supporting information). This results in a concomitant reduction of the shift between the states in the two MoS2 layers to 0.2 eV. In passing, we note that in all our simulations we assumed a defect-free MoS_2 layer, which is not necessarily the case in all experiments. Defects changing the position of the Fermi level and potentially also providing localized interaction sites can, for example, trigger much more significant charge rearrangements between strongly S-deficient MoS_2 layers and TiOPc molecules, as recently discussed by Park *et al* [38]. The above considerations, however, show that as long as these charge rearrangements are largely symmetric between the molecular layer and the two MoS_2 sheets, this would not significantly change the electrostatic shifts.

Another interesting observation in figure 3 is that there are no significant local potential variations induced by the TiOPc layer, which extend into the MoS_2 sheets. This is associated with screening within the MoS_2 layers, as can be inferred from a comparison between the electrostatic energy shown in figure 3 with that of a hypothetical free-standing TiOPc layer in the absence of the 2D semiconductors (see supporting information).

To more clearly visualize the spatial distribution of the states of the MoS_2|TiOPc|MoS_2 system, a contour map of the local density of states (LDOS) as a function of the position along the stacking direction is contained in figure 4. It shows how the electronic states in the system are distributed as a function of energy and position in stacking direction. The data not only confirm the type II band alignment of the MoS_2 layers, but also clearly show that the largest contribution to the DOS at the band edges stems from regions close to the transition metal (molybdenum for this system) [37, 39–41], together with contributions from the

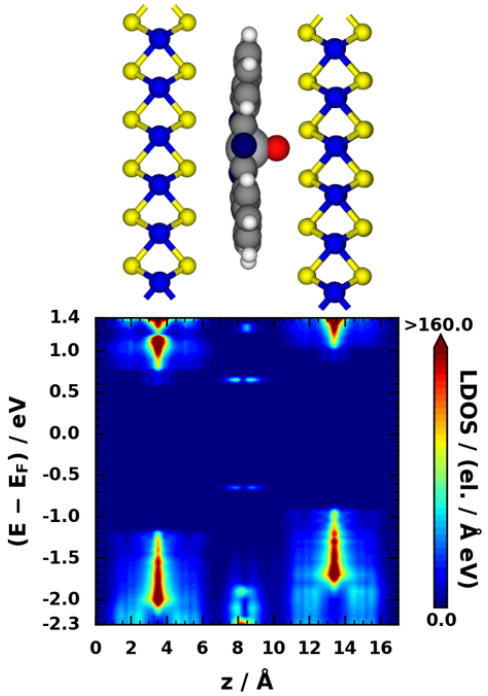

Figure 4. Local density of states (LDOS) of the MoS_2|TiOPc|MoS_2 heterostructure spatially resolved with respect to the stacking direction (i.e. integrated over the unit cell in the plane perpendicular to it). The Fermi energy is set to the middle of the band gap of the heterostructure.

sulfur atoms. The densities of states projected onto the individual species of the MoS_2 layers further resolved according to their orbital angular momentum can be found in the supporting information.

PDOS and LDOS plots show that the occupied states of the TiOPc layer lie in the gap of both MoS_2 layers (similar to what has been found for ZnPc on MoS_2) [42]. This observation is very likely not a methodological artefact, as it prevails when reducing the self-interaction error in the DFT calculations by employing hybrid functionals [43, 44] (see supporting information). For TiOPc intercalation, these intra-gap states are π-states corresponding to the molecular frontier orbitals localized nearly exclusively on the C atoms (for the HOMO) and on the C and N atoms (for the LUMO). This can be concluded from a comparison between calculated molecular orbital shapes and the local densities of states in the periodic stack as well as from atom-projected DOSs of the intra-gap features (see supporting information). Electronic states of the intercalated molecules in the TMD gaps could lead to trap states especially for electrons and holes, which would be detrimental for applications in optoelectronic devices geared at splitting excitons into free electrons and holes (like photodetectors or solar cells). In practice this problem can be, however, overcome by choosing dipolar molecules with larger ionization energies and gaps, provided that the molecules are designed such that they still align with dipoles parallel to the stacking direction.

2.3. More complex quantum-structures: cascades and wells

The idea of using collective electrostatic effects to shift the electronic states in vdW heterostructures can be extended to more complex systems containing more than two TMD layers in combination with intercalated molecular layers with identical or opposing dipole orientations. In this way, for example, quantum cascades and quantum wells can be created: Having parallel dipole arrangements in successive polar layers (as shown schematically in figure 5(a)) results in a cascade of electronic states [24]. This is illustrated by the LDOSs of a correspondingly designed 3-layer stack in figure 5(b). The cascade creates a situation interesting for spatially separating electrons and holes.

Upon reversing the dipole orientation in one of the polar films, the situation shown in figures 5(c) and (d) is achieved. For the dipole orientations considered here, this would lead to an accumulation of holes in the central TMD layer. In practice, such a structure could possibly be realized by stacking a TMD layer (containing adsorbed polar molecules) in a 'face down' fashion onto a two-layer stack. In passing we note that due to the 'robust' conceptual nature of the electrostatic design approach, a slip or rotation of consecutive layers should not adversely affect the electronic structure of the stack.

Notably, for the examples shown in figure 5 we employed molecular systems with identical dipole moments for both intercalated layers; as an alternative, locally varying step sizes can be realized using molecular layers with different dipole densities. Moreover, one is not restricted to only three layers, which implies that conceptually there is no limit to the complexity of electronic structure of the systems that can be realized employing electrostatic design.

2.4. Electrostatically designed heterobilayers

So far only systems containing chemically identical TMD layers have been described. When extending the discussion to heterogeneous stacks, in the simulations we are restricted to the combination of materials with very similar lattice constants, due to the employed periodic boundary conditions. Otherwise, considerable strain would have to be applied to the layers in order to study the heterostructure in reasonably small unit cells. This would blur the picture, because even small amounts of strain can significantly change the electronic structure of TMDs [45]. Interestingly, for WSe_2 and $MoSe_2$ the calculated lattice constants match within 0.08%. Thus a simple unit cell containing only one TiOPc molecule can be constructed. For this construction the lattice constant of the lower layer (WSe_2 in this case) has been used. Due to the very low lattice mismatch the effects of strain on the $MoSe_2$ layer are negligible. WSe_2|$MoSe_2$ bilayer systems are interesting also from an application point of view, as they have been used in solar cells [46] and interlayer exciton optoelectronics [47, 48].

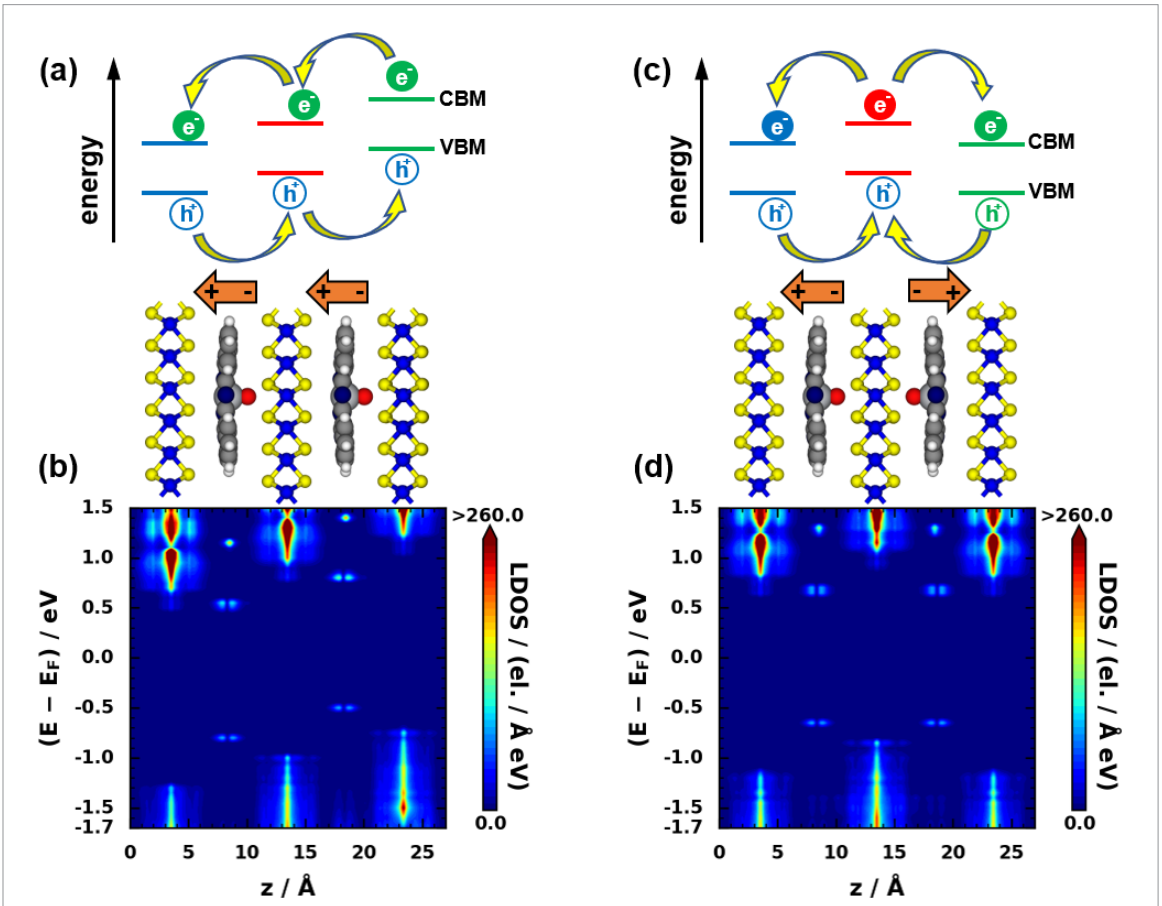

Figure 5. Schematic representation and local density of states (LDOS) of quantum cascades ((a) and (b)) and quantum wells (c) and (d). The LDOS is spatially resolved with respect to the stacking direction. The Fermi energy is set to the middle of the band gap.

The $WSe_2|MoSe_2$ bilayer displays type II band alignment [36, 48–53] with band offsets of 0.30 eV for the valence [50] and 0.45 eV for the conduction-band [54] edges (where the valence-band offset is taken from angular resolved photoelectron spectroscopy experiment and the conduction-band offset is derived from GW calculations). As these values are in the range of the shifts induced electrostatically by the TiOPc layers discussed above, we tested, whether electrostatic design can be used to qualitatively change the system from type II to type I band alignment. The PDOSs of the relevant systems are shown in figure 6. For the bonded $WSe_2|MoSe_2$ bilayer (figure 6(a)), type II band alignment is indeed obtained, but with smaller band offsets than reported in experiment [50] and in previous theoretical studies [11, 54]. The latter is very likely a consequence of differing interlayer distances. They, on the one hand, depend on the stacking motif of consecutive TMD layers. On the other hand, the interlayer distance in the simulations is influenced by the choice of the van der Waals correction scheme. In the experiments it is impacted by organic residues trapped between successive TMD layers [55]. The situation displayed in figure 6(a) is obtained for C7 (2H) stacking, which is the lowest energy configuration in our calculations (in agreement with the calculations of Zhang *et al*) [56]. It is also the stacking motif of $MoSe_2$ and WSe_2 in bulk crystals [57, 58]. For AA stacking with coplanar layers and a slightly increased interlayer distance the valence band offset is larger (approximately 0.2 eV; see supporting information for details). Consistently, when reducing the interlayer electronic coupling by positioning the layers at the distance they will eventually adopt in the TiOPc-intercalated situation, the energetic offsets of the band edges increase even more (to 0.2 eV for the valence band edges and to 0.3 eV for the conduction band edges, see figure 6(b)).

Again, the situation changes qualitatively when including the TiOPc molecules in the simulations: the electrostatically induced shift of the electronic states between the WSe_2 and $MoSe_2$ due to the presence of the molecular layer amounts to 0.25 eV. Consequently, the conduction band edge of $MoSe_2$ still lies below that of WSe_2, while for the valence band edges that of WSe_2 is lower. In this way, a situation with type I band alignment is realized (figure 6(c)). Conversely, when reversing the stacking order while maintaining the TiOPc orientation (figure 6(d)), particularly large type II offsets are achieved.

Finally, we note that the concept of electrostatic design of vdW heterostructures is not restricted to stacks consisting of semiconducting TMD layers, but also prevails for example for stacks of graphene sheets. Corresponding data are presented in the supporting information.

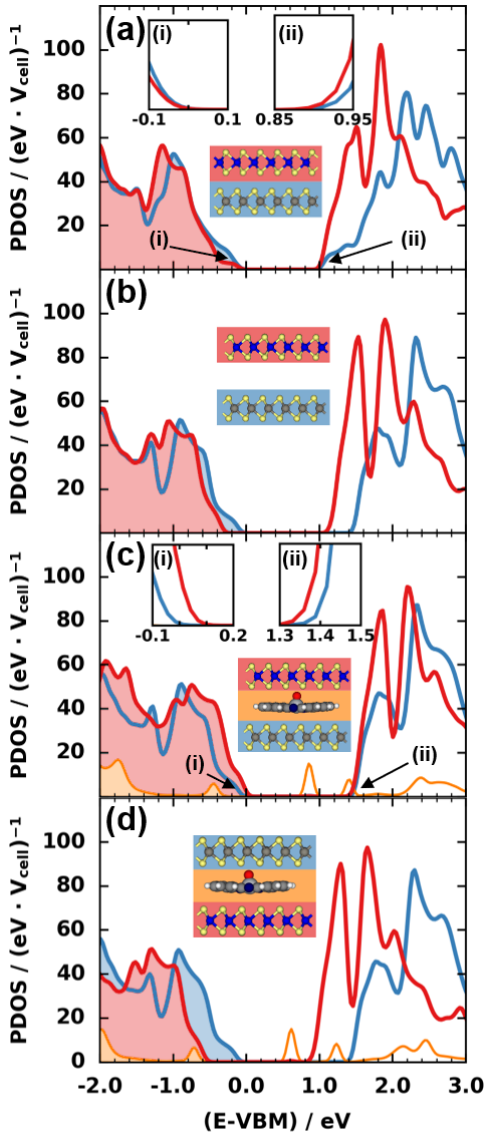

Figure 6. Density of states projected onto the different layers in the WSe_2|TiOPc|$MoSe_2$ (blue|orange|red) system (a) for the heterobilayer, (b) for WSe_2 and $MoSe_2$ layers arranged in the same geometry as in the intercalated stack (but in the absence of TiOPc molecules), (c) in the stack containing a monolayer of dipolar TiOPc molecules and (d) in the stack with the order of the TMD layers reversed ($MoSe_2$|TiOPc|WSe_2). All energies are plotted relative to the valence band maximum of the WSe_2 layer for the sake of consistency; all shaded electronic states are occupied in the calculations (with details regarding the employed occupation smearing described in the Methods section). The structures of the considered stacks are shown as insets; they have been fully optimized for the systems depicted in panels (a), (c) and (d). Additional insets in (a) and (c) show a zoom into the regions of the valence and conduction band edges.

2.5. Dielectric screening and band-gap renormalization

It has been demonstrated that band-gaps and exciton binding energies of semiconducting TMDs depend strongly on the surrounding dielectric environment [59–62]. To quantify these effects, one has to go beyond the single particle picture using methods like GW [63]. Such calculations, for instance, reveal that, when comparing a freestanding MoS_2 monolayer in vacuum to a MoS_2 layer sandwiched between two dielectrics with a dielectric constant of 5, the gap is reduced by approximately 24% [60]. Within the bandgap center alignment scheme [64], this affects the positions of the conduction and valence band edges equivalently, as one assumes a quantitatively similar effect of the self-energy correction on the VBM and the CBM (albeit with different signs) [65, 66]. This assumption has been shown to hold for molybdenum and tungsten based dichalcogenides when using GW calculations [64]. On the basis of these findings we conclude that in simple heterostructures, like MoS_2|TiOPc|MoS_2, interlayer screening should have no significant effect on the TiOPc-induced changes of the band alignment, since in such systems both MoS_2 layers feel a similar dielectric environment. Only the energy of the transport gap decreases and the exciton binding energy is reduced compared to an isolated monolayer. However, it still remains one order of magnitude larger than in conventional 3D semiconductors—at least for $MoSe_2$ on bilayer graphene and HOPG (the systems investigated in [59]). These considerations show that for stacks like MoS_2|TiOPc|MoS_2, screening and excitonic effects are certainly relevant for their detailed optical properties, but should not significantly impact the modifications of the electronic structure arising from the electrostatic design idea presented in the present paper. Similar considerations apply to heterostructures consisting of different transition metal dichalcogenide layers provided that their dielectric constants are not dramatically different [67].

In cases, where the two TMD layers feel different dielectric environments [61, 62], e.g. because the vdW stack is deposited onto a (dielectric) substrate, or the TMD layers themselves have significantly different dielectric constants, stacks with type I and type II band alignment are affected differently: for heterostructures with type II band alignment non-symmetric dielectric environments will result in the increase of one of the band offsets and a decrease of the other (see figures 7(a)–(c)). In the type I case, both band offsets are either increased or decreased, depending on which layer faces the environment with a higher dielectric constant (see figures 7(d)–(f)).

For the quantum cascade and the quantum well structures, the situation is somewhat more involved, since there (in the absence of a dielectric surrounding), the band gap renormalization will be larger for the central layer compared to the outer ones. For the quantum cascade shown in figures 5(a) and (b), this effect leads to an increase of the valence band offset between the first and the second MoS_2 layer and to a decrease of the corresponding conduction band, while for the interface between the second and third MoS_2 layer the opposite happens (for a corresponding figure see supporting information). For the quantum well in figures 5(c) and (d), the result is an increase in the depth of the well for holes while the band offset for the electrons is decreased. Based on the data by Ryou *et al* [60] one can derive a rough estimate for the mag-

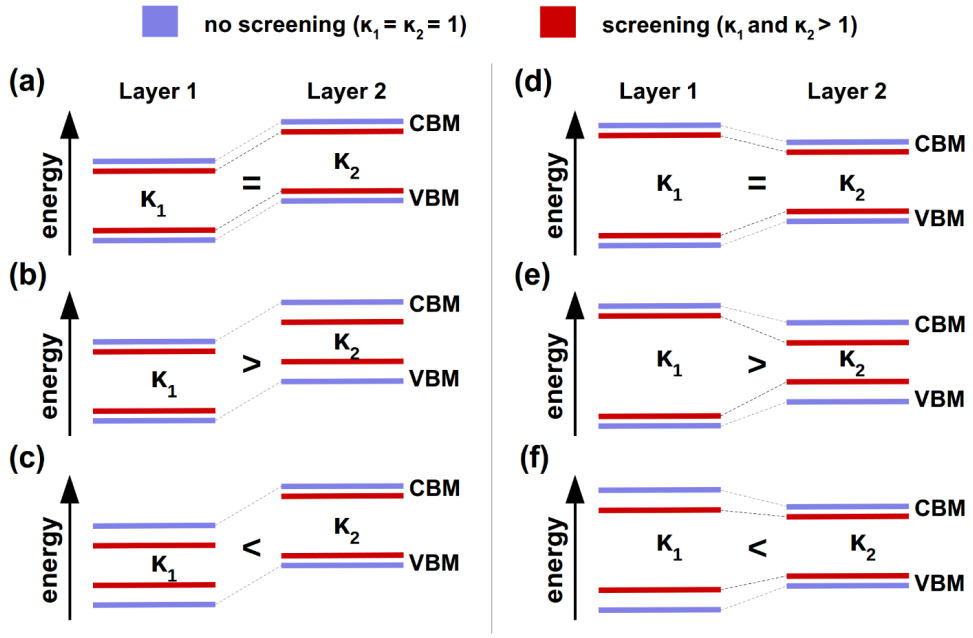

Figure 7. Changes of the bandgap and the band alignment in a vdW heterobilayer with type II ((a)–(c)) and type I ((d)–(f)) band alignment. These changes depend on the effective dielectric constants κ_1 and κ_2 of each layer, which represent the dielectric surrounding felt by the respectively other layer. The band extrema (VBM and CBM) are colored in red (blue) when considering (not considering) screening.

nitude of that effect: assuming that the outer MoS_2 layers are facing vacuum on one side, and the rest of the heterostructure on the other side and that all the MoS_2 layers have the same effective dielectric constant (here we take κ_E equal to 10, to obtain an upper boundary), the difference in band-gap renormalization between the central and the outer MoS_2 layers amounts to 0.2 eV. In the framework of the bandgap center alignment scheme, this results in changes of the level alignment by 0.1 eV (for more details see supporting information).

3. Conclusions

In conclusion, our calculations reveal that applying electrostatic design to van der Waals heterostructures is a viable way to tune the electronic structure of such systems. Especially the band alignment of successive TMD layers can be changed via the insertion of ordered polar molecular layers. The suggested approach also allows the realization of more complex heterostructures and a change of the type of band-alignment. From a practical point of view, it will be necessary in the future to explore strategies for stabilizing the intercalated layers either through crosslinking between molecules or through direct bonding the dipolar molecules to the TMD layers. Nevertheless, the versatility of electronic properties that can be realized by combining the presented approach with the huge pool of available layered materials to be stacked into vdW heterostructure is enormous and appears to be limited only by the imagination of the materials' designer.

4. Methods

4.1. DFT calculations

All calculations are performed using density functional theory (DFT) as implemented in the FHI-aims package [68]. The exchange and correlation part is treated using the PBE functional [69]. A k-point grid of 8 × 8 × 1 is employed. Regarding the basis set, 'tight' settings with full 'tier2' for all included atomic species have been used. Van der Waals interactions are considered based on the pairwise correction scheme proposed by Tkatchenko and Scheffler [70]. The occupation of the Kohn–Sham eigenstates was modelled by applying a Gaussian broadening function [71] with a width of 0.01 eV. Details on the convergence settings of the self-consistent field procedure and of the geometry optimization can be found in the supporting information. Spin–orbit coupling (SOC) is not considered in our calculations, as it is not important for the effects discussed in this paper and calculations including SOC would be very memory intensive and, thus, computationally expensive. Ovito [72] and Mayavi [73] were used for graphical visualization.

4.2. Geometric details of the heterostructures

The lateral arrangement of the TiOPc molecules in the above considerations is again inspired by the situation on HOPG: there, for a CuPc monolayer Wang *et al* [74] found a square unit cell containing one molecule with a lattice constant of 13.8 Å. This unit cell cannot be directly adopted in our calculations, as a square unit cell is incompatible

with the hexagonal symmetry of the MoS_2 substrate. As even minor (unidirectional) strain would significantly modify the properties of the TMDs (e.g. triggering a direct to indirect gap transition [45]), we fully relaxed the substrate and then picked the smallest rectangular supercell, which was large enough to accommodate a single TiOPc molecule. The only expected impact on the properties of the resulting minor distortion of the TiOPc layer is a minute decrease of the dipole density, which has no relevant consequences for the presented considerations. The supporting information contains a detailed description of the structure of the resulting unit cell, the strategy employed to set-up and optimize the structures of the quantum cascades, quantum wells, and heterobilayers, and a compilation of the resulting structures.

Acknowledgments

We thank K Bolotin for stimulating discussions and O T Hofmann for providing continuous support when performing the simulations. We are grateful for financial support by the Austrian Science Fund (FWF): P28051-N36 and by the European Union Seventh Framework Programme Initial Training Network THINFACE under grant agreement 607232. Electronic structure calculations have been performed using the Vienna Scientific Cluster.

Associated content

The Supporting Information is available free of charge and contains: computational details, and details on the system set-up and optimization; densities of states of isolated monolayers and for $WSe_2|MoSe_2$ heterobilayers for different stacking motifs; band structures of the van der Waals heterostructures and the individual sub-systems and of the MoS_2 homobilayer; DOSs for the hybrid-functional calculation and for electrostatically designed graphene stacks; species- and orbital angular momentum projected DOSs; charge rearrangements and bond dipole of the $MoS_2|TiOPc|MoS_2$ heterostructure with the top MoS_2 layer being (not) lifted; comparison of the electrostatic energy generated by the TiOPc layer in the absence, respectively, presence of the MoS_2 sheets; species-projected and angular momentum resolved DOS of the TiOPc layer as well as the LDOS of the intra-gap states and the corresponding molecular orbitals; species-projected DOS of the MoS_2 bilayer; depictions of the relaxed geometries; details regarding the quantitative effect of dielectric screening in the quantum cascades and wells.

Notes

The authors declare no competing financial interest

Author contributions

CW performed all calculations presented in the paper, evaluated and interpreted the data, and wrote a first draft of the manuscript. SSH supported the simulations, contributed to the general setting-up of the project, and revised the manuscript. EZ conceived the project idea, steered the work, and significantly contributed to the interpretation of the data and the writing of the manuscript.

ORCID iDs

Christian Winkler https://orcid.org/0000-0002-7463-6840
Shashank S Harivyasi https://orcid.org/0000-0002-2174-5226
Egbert Zojer https://orcid.org/0000-0002-6502-1721

References

[1] Novoselov K S, Geim A K, Morozov S V, Jiang D, Zhang Y, Dubonos S V, Grigorieva I V and Firsov A A 2004 Electric field effect in atomically thin carbon films *Science* **306** 666–9
[2] Xiao D, Liu G-B, Feng W, Xu X and Yao W 2012 Coupled spin and valley physics in monolayers of MoS_2 and other group-VI dichalcogenides *Phys. Rev. Lett.* **108** 196802
[3] Xu X, Yao W, Xiao D and Heinz T F 2014 Spin and pseudospins in layered transition metal dichalcogenides *Nat. Phys.* **10** 343–50
[4] Mak K F, McGill K L, Park J and McEuen P L 2014 The valley Hall effect in MoS_2 transistors *Science* **344** 1489–92
[5] Britnell L *et al* 2013 Strong light–matter interactions in heterostructures of atomically thin films *Science* **340** 1311–4
[6] Wurstbauer U, Miller B, Parzinger E and Holleitner A W 2017 Light–matter interaction in transition metal dichalcogenides and their heterostructures *J. Phys. D: Appl. Phys.* **50** 173001
[7] Zhang C, Wang H, Chan W, Manolatou C and Rana F 2014 Absorption of light by excitons and trions in monolayers of metal dichalcogenide MoS_2: experiments and theory *Phys. Rev. B* **89** 205436
[8] Song Z *et al* 2017 Electronic properties of a 1D intrinsic/p-doped heterojunction in a 2D transition metal dichalcogenide semiconductor *ACS Nano* **11** 9128–35
[9] Peimyoo N, Yang W, Shang J, Shen X, Wang Y and Yu T 2014 Chemically driven tunable light emission of charged and neutral excitons in monolayer WS_2 *ACS Nano* **8** 11320–9
[10] Zheng Y J *et al* 2016 Heterointerface screening effects between organic monolayers and monolayer transition metal dichalcogenides *ACS Nano* **10** 2476–84
[11] Rasmussen F A and Thygesen K S 2015 Computational 2D materials database: electronic structure of transition-metal dichalcogenides and oxides *J. Phys. Chem. C* **119** 13169–83
[12] Ye Z, Cao T, O'Brien K, Zhu H, Yin X, Wang Y, Louie S G and Zhang X 2014 Probing excitonic dark states in single-layer tungsten disulphide *Nature* **513** 214–8
[13] He K, Kumar N, Zhao L, Wang Z, Mak K F, Zhao H and Shan J 2014 Tightly bound excitons in monolayer WSe_2 *Phys. Rev. Lett.* **113** 026803
[14] Chernikov A, Berkelbach T C, Hill H M, Rigosi A, Li Y, Aslan O B, Reichman D R, Hybertsen M S and Heinz T F 2014 Exciton binding energy and nonhydrogenic Rydberg series in monolayer WS_2 *Phys. Rev. Lett.* **113** 073802
[15] Withers F *et al* 2015 Light-emitting diodes by band-structure engineering in van der Waals heterostructures *Nat. Mater.* **14** 301–6

[16] Mak K F, Lee C, Hone J, Shan J and Heinz T F 2010 Atomically thin MoS_2: a new direct-gap semiconductor *Phys. Rev. Lett.* **105** 136805

[17] Wang Q H, Kalantar-Zadeh K, Kis A, Coleman J N and Strano M S 2012 Electronics and optoelectronics of two-dimensional transition metal dichalcogenides *Nat. Nanotechnol.* **7** 699–712

[18] Zhang W, Wang Q, Chen Y, Wang Z and Wee A T S 2016 Van der Waals stacked 2D layered materials for optoelectronics *2D Mater.* **3** 22001

[19] Wang X and Xia F 2015 Van der Waals heterostructures: stacked 2D materials shed light *Nat. Mater.* **14** 264–5

[20] Geim A K and Grigorieva I V 2013 Van der Waals heterostructures *Nature* **499** 419–25

[21] He Q, Zeng Z, Yin Z, Li H, Wu S, Huang X and Zhang H 2012 Fabrication of flexible MoS_2 thin-film transistor arrays for practical gas-sensing applications *Small* **8** 2994–9

[22] Pu J, Yomogida Y, Liu K-K, Li L-J, Iwasa Y and Takenobu T 2012 Highly Flexible MoS_2 thin-film transistors with ion gel dielectrics *Nano Lett.* **12** 4013–7

[23] Miró P, Audiffred M and Heine T 2014 An atlas of two-dimensional materials *Chem. Soc. Rev.* **43** 6537

[24] Kretz B, Egger D A and Zojer E 2015 A toolbox for controlling the energetics and localization of electronic states in self-assembled organic monolayers *Adv. Sci.* **2** 1400016

[25] Kraberger G J, Egger D A and Zojer E 2015 Tuning the electronic structure of graphene through collective electrostatic effects *Adv. Mater. Interfaces* **2** 1500323

[26] Heimel G, Rissner F and Zojer E 2010 Modeling the electronic properties of π-conjugated self-assembled monolayers *Adv. Mater.* **22** 2494–513

[27] Natan A, Kronik L, Haick H and Tung R T 2007 Electrostatic properties of ideal and non-ideal polar organic monolayers: implications for electronic devices *Adv. Mater.* **19** 4103–17

[28] Natan A, Zidon Y, Shapira Y and Kronik L 2006 Cooperative effects and dipole formation at semiconductor and self-assembled-monolayer interfaces *Phys. Rev.* B **73** 193310

[29] Cahen D, Naaman R and Vager Z 2005 The cooperative molecular field effect *Adv. Funct. Mater.* **15** 1571–8

[30] Monti O L A 2012 Understanding interfacial electronic structure and charge transfer: an electrostatic perspective *J. Phys. Chem. Lett.* **3** 2342–51

[31] Abu-Husein T, Schuster S, Egger D A, Kind M, Santowski T, Wiesner A, Chiechi R, Zojer E, Terfort A and Zharnikov M 2015 The effects of embedded dipoles in aromatic self-assembled monolayers *Adv. Funct. Mater.* **25** 3943–57

[32] Fukagawa H, Yamane H, Kera S, Okudaira K K and Ueno N 2006 Experimental estimation of the electric dipole moment and polarizability of titanyl phthalocyanine using ultraviolet photoelectron spectroscopy *Phys. Rev.* B **73** 041302

[33] Dean C R *et al* 2010 Boron nitride substrates for high-quality graphene electronics *Nat. Nanotechnol.* **5** 722–6

[34] Chiu M H, Li M Y, Zhang W, Hsu W T, Chang W H, Terrones M, Terrones H and Li L J 2014 Spectroscopic signatures for interlayer coupling in MoS_2–WSe_2 van der waals stacking *ACS Nano* **8** 9649–56

[35] Zhang C, Chuu C-P, Ren X, Li M-Y, Li L-J, Jin C, Chou M-Y and Shih C-K 2017 Interlayer couplings, Moiré patterns, and 2D electronic superlattices in MoS_2/WSe_2 hetero-bilayers *Sci. Adv.* **3** e1601459

[36] Kosmider K and Fernández-Rossier J 2013 Electronic properties of the MoS_2–WS_2 heterojunction *Phys. Rev.* B **87** 75451

[37] Padilha J E, Peelaers H, Janotti A and Van De Walle C G 2014 Nature and evolution of the band-edge states in MoS_2: from monolayer to bulk *Phys. Rev.* B **90** 205420

[38] Park J H *et al* 2017 Defect passivation of transition metal dichalcogenides via a charge transfer van der Waals interface *Sci. Adv.* **3** e1701661

[39] Lu S-C and Leburton J-P 2014 Electronic structures of defects and magnetic impurities in MoS_2 monolayers *Nanoscale Res. Lett.* **9** 676

[40] Su X, Ju W, Zhang R, Guo C, Zheng J, Yong Y and Li X 2016 Bandgap engineering of MoS_2/MX_2 (MX_2 = WS_2, $MoSe_2$ and WSe_2) heterobilayers subjected to biaxial strain and normal compressive strain *RSC Adv.* **6** 18319–25

[41] Kadantsev E S and Hawrylak P 2012 Electronic structure of a single MoS_2 monolayer *Solid State Commun.* **152** 909–13

[42] Kafle T R, Kattel B, Lane S D, Wang T, Zhao H and Chan W-L 2017 Charge transfer exciton and spin flipping at organic-transition metal dichalcogenide interfaces *ACS Nano* **11** 10184–92

[43] Perdew J P and Zunger A 1981 Self-interaction correction to density-functional approximations for many-electron systems *Phys. Rev.* B **23** 5048–79

[44] Adamo C and Barone V 1999 Toward reliable density functional methods without adjustable parameters: the PBE0 model *J. Chem. Phys.* **110** 6158–70

[45] Yun W S, Han S W, Hong S C, Kim I G and Lee J D 2012 Thickness and strain effects on electronic structures of transition metal dichalcogenides: 2H-MX_2 semiconductors (M = Mo, W; X = S, Se, Te) *Phys. Rev.* B **85** 33305

[46] Gong Y *et al* 2015 Two-step growth of two-dimensional WSe_2/$MoSe_2$ heterostructures *Nano Lett.* **15** 6135–41

[47] Ross J S *et al* 2017 Interlayer exciton optoelectronics in a 2D heterostructure *p-n* junction *Nano Lett.* **17** 638–43

[48] Chiu M-H, Zhang C, Shiu H-W, Chuu C-P, Chen C-H, Chang C-Y S, Chen C-H, Chou M-Y, Shih C-K and Li L-J 2015 Determination of band alignment in the single-layer MoS_2/WSe_2 heterojunction *Nat. Commun.* **6** 7666

[49] Kang J, Tongay S, Zhou J, Li J and Wu J 2013 Band offsets and heterostructures of two-dimensional semiconductors *Appl. Phys. Lett.* **102** 12111

[50] Wilson N R *et al* 2017 Determination of band offsets, hybridization, and exciton binding in 2D semiconductor heterostructures *Sci. Adv.* **3** e1601832

[51] Rivera P *et al* 2015 Observation of long-lived interlayer excitons in monolayer $MoSe_2$–WSe_2 heterostructures *Nat. Commun.* **6** 6242

[52] Özçelik V O, Azadani J G, Yang C, Koester S J and Low T 2016 Band alignment of two-dimensional semiconductors for designing heterostructures with momentum space matching *Phys. Rev.* B **94** 035125

[53] Terrones H, López-Urías F and Terrones M 2013 Novel hetero-layered materials with tunable direct band gaps by sandwiching different metal disulfides and diselenides *Sci. Rep.* **3** 1549

[54] Zhang C *et al* 2017 Systematic study of electronic structure and band alignment of monolayer transition metal dichalcogenides in Van der Waals heterostructures *2D Mater.* **4** 15026

[55] Alexeev E M *et al* 2017 Imaging of interlayer coupling in van der Waals heterostructures using a bright-field optical microscope *Nano Lett.* **17** 5342–9

[56] Zhang F, Li W, Dai X, Li W and Dai X 2017 Modulation of electronic structures of $MoSe_2$/WSe_2 van der Waals heterostructure by external electric field *Solid State Commun.* **266** 11–5

[57] James P B and Lavik M T 1963 The crystal structure of $MoSe_2$ *Acta Crystallogr.* **16** 1183

[58] Schutte W J, De Boer J L and Jellinek F 1987 Crystal structures of tungsten disulfide and diselenide *J. Solid State Chem.* **70** 207–9

[59] Ugeda M M *et al* 2014 Giant bandgap renormalization and excitonic effects in a monolayer transition metal dichalcogenide semiconductor *Nat. Mater.* **13** 1091–5

[60] Ryou J, Kim Y-S, Santosh K C and Cho K 2016 Monolayer MoS_2 bandgap modulation by dielectric environments and tunable bandgap transistors *Sci. Rep.* **6** 29184

[61] Thygesen K S 2017 Calculating excitons, plasmons, and quasiparticles in 2D materials and van der Waals heterostructures *2D Mater.* **4** 22004

[62] Latini S, Winther K T, Olsen T and Thygesen K S 2017 Interlayer excitons and band alignment in MoS_2/hBN/WSe_2 van der Waals heterostructures *Nano Lett.* **17** 938–45

[63] Hedin L 1965 New method for calculating the one-particle Green's function with application to the electron-gas problem *Phys. Rev.* **139** A796–823
[64] Liang Y, Huang S, Soklaski R and Yang L 2013 Quasiparticle band-edge energy and band offsets of monolayer of molybdenum and tungsten chalcogenides *Appl. Phys. Lett.* **103** 42106
[65] Toroker M C, Kanan D K, Alidoust N, Isseroff L Y, Liao P and Carter E A 2011 First principles scheme to evaluate band edge positions in potential transition metal oxide photocatalysts and photoelectrodes *Phys. Chem. Chem. Phys.* **13** 16644
[66] Jiang H 2012 Electronic band structures of molybdenum and tungsten dichalcogenides by the *GW* approach *J. Phys. Chem.* C **116** 7664–71
[67] Andersen K, Latini S and Thygesen K S 2015 Dielectric genome of van der Waals heterostructures *Nano Lett.* **15** 4616–21
[68] Blum V, Gehrke R, Hanke F, Havu P, Havu V, Ren X, Reuter K and Scheffler M 2009 *Ab initio* molecular simulations with numeric atom-centered orbitals *Comput. Phys. Commun.* **180** 2175–96
[69] Perdew J P, Burke K and Ernzerhof M 1996 Generalized gradient approximation made simple *Phys. Rev. Lett.* **77** 3865–8
[70] Tkatchenko A and Scheffler M 2009 Accurate molecular Van Der Waals interactions from ground-state electron density and free-atom reference data *Phys. Rev. Lett.* **102** 73005
[71] Fu C L and Ho K M 1983 First-principles calculation of the equilibrium ground-state properties of transition metals: applications to Nb and Mo *Phys. Rev.* B **28** 5480–6
[72] Stukowski A 2010 Visualization and analysis of atomistic simulation data with OVITO–the open visualization tool *Model. Simul. Mater. Sci. Eng.* **18** 15012
[73] Ramachandran P and Varoquaux G 2011 Mayavi: 3D visualization of scientific data *Comput. Sci. Eng.* **13** 40–51
[74] Wang S D, Dong X, Lee C S and Lee S T 2004 Orderly growth of copper phthalocyanine on highly oriented pyrolytic graphite (HOPG) at high substrate temperatures *J. Phys. Chem.* B **108** 1529–32